Catalysis Today 147S (2009) S191–S197

Contents lists available at ScienceDirect

Catalysis Today

journal homepage: www.elsevier.com/locate/cattod

WGS reaction over nanostructured $CuO–CeO_2$ catalysts prepared by hard template method: Characterization, activity and deactivation

Petar Djinović [a], Jurka Batista [a], Albin Pintar [a,b,*]

[a] National Institute of Chemistry, P.O. Box 660, SI-1001 Ljubljana, Slovenia
[b] Faculty of Chemistry and Chemical Technology, University of Ljubljana, P.O. Box 537, SI-1001 Ljubljana, Slovenia

ARTICLE INFO

Article history:
Available online 31 July 2009

Keywords:
$CuO–CeO_2$ catalysts
Hard template method
WGS reaction
Carbonates
Catalyst deactivation

ABSTRACT

This study focuses on water–gas shift reaction (WGSR) activity of $CuO–CeO_2$ catalysts containing 10, 15 and 20 mol% CuO synthesized by hard template method with KIT-6 silica acting as a template. The obtained solids were characterized by N_2 adsorption/desorption, XRD, H_2-TPR/TPD, N_2O decomposition, *in situ* DRIFTS and NH_3 chemisorption/TPD methods. The catalysts exhibited ordered mesoporous structure, which was identified as the negative replica of KIT-6 silica pore system with CuO dispersion values between 28 and 40%. H_2-TPR/TPD experiments revealed facile and extensive CeO_2 reduction in tested samples, which increased with CuO loading, indicating strong interactions between both oxide phases. On the other hand, abundance of surface acidic sites decreased with increasing CuO content. WGS reaction activity was tested at the stoichiometric CO/H_2O ratio and low contact times in the temperature range from 250 to 450 °C. At reaction temperatures above 375 °C, catalyst deactivation was observed, regardless of CuO content. Despite rigorous reaction conditions, CO conversion up to 62% was attained, with H_2 selectivity above 99% in the entire temperature range.

1. Introduction

$CuO–CeO_2$ catalysts exhibit high activity for a number of heterogeneously catalyzed reactions, including WGS [1,2], PROX [3–5], NO removal from automotive exhaust gasses [6] and methanol steam reforming [7]. Some of these reactions are of very high technological importance with regard to pure H_2 production, either for use as fuel or for synthesis of value added products. Since H_2 is considered as a green fuel of the future and its global demand grows annually, synthesis of more active and selective catalysts for its production from various feedstocks is experiencing a steep rise in the last decade. Activity of $CuO–CeO_2$ catalysts in the above-mentioned reactions stems from strong interactions between CuO and CeO_2 phases, which influences the creation of defects (oxygen vacancies) by facile interplay between $Cu^{2+} \leftrightarrow Cu^{1+}$ and $Ce^{4+} \leftrightarrow Ce^{3+}$ redox couples. Catalyst active sites are very often contributed to the $CuO–CeO_2$ interface area, which can be maximized over nanocrystalline CeO_2 with very high specific area and highly dispersed CuO [8,9].

One way of increasing BET surface area of $CuO–CeO_2$ catalysts and improve CuO dispersion is the use of hard template preparation method [8,10]. By using a thermally stable template with very high porosity and ordered arrays of mesopores, which is impregnated with a metal salt solution and leached after precursor mineralization, catalysts with very high surface area can be obtained, which usually cannot be prepared by conventional methods [11]. Mesoporous $CuO–CeO_2$ catalysts synthesized following this procedure are composed of nanocrystalline CeO_2 frameworks with high similarities to the silica template pore system and exhibit remarkable stability in air at temperatures as high as 700 °C [11]. In this work, we report on the characterization, WGSR activity and stability of $CuO–CeO_2$ catalysts with nominal 10, 15 and 20 mol% CuO loadings. WGSR activity was tested in the temperature range between 250 and 450 °C, low contact times and high CO and H_2O concentrations. Influence of CO_2 addition to the feed gas stream was also evaluated in terms of catalyst activity and deactivation.

2. Experimental

$CuO–CeO_2$ catalysts with nominal 10, 15 and 20 mol% CuO content were synthesized by hard template method using KIT-6 silica as a template. Detailed information regarding KIT-6 silica synthesis can be found elsewhere [8,10]. Appropriate amounts of

* Corresponding author at: National Institute of Chemistry, P.O. Box 660, SI-1001 Ljubljana, Slovenia. Tel.: +386 1 47 60 237; fax: +386 1 47 60 300.
E-mail address: albin.pintar@ki.si (A. Pintar).

0920-5861/$ – see front matter © 2009 Elsevier B.V. All rights reserved.
doi:10.1016/j.cattod.2009.07.009

$Cu(NO_3)_2{\cdot}3H_2O$ (99.5% purity, Merck) and $Ce(NO_3)_3{\cdot}6H_2O$ (99% purity, Aldrich) were dissolved in 25 ml of ethanol (absolute, p.a., Riedel-de Haën). The amounts of added metal salts were calculated to yield a total metal ion concentration of 0.7 M. Higher concentrations of metal salts are reported to induce formation of bulk oxide particles on the outer surface of silica [12]. Into 15 ml of this solution, 1 g of KIT-6 was added and stirred at room temperature for 1 h. The impregnated template was dried overnight at 60 °C. The obtained CuCe15 catalyst precursor was heated in an oven at 400 °C for 3 h to completely decompose nitrate species. CuCe10 and CuCe20 precursors were calcined at 550 and 450 °C, respectively. The impregnation step was repeated with 10 ml of the remaining ethanol–metal salt mixture. After overnight drying at 60 °C, CuCe15 precursor was again calcined at 400 °C (CuCe10 at 550 °C and CuCe20 at 450 °C) for 3 h. In our previous work [13], an influence of calcination temperature (ranging from 400 to 850 °C, raised in 50 °C increments) on sintering, agglomeration and loss of CuO dispersion, change in redox properties and acid site abundance was investigated for $CuO–CeO_2$ catalysts and correlated to activity in WGS reaction. It was discovered that elevated calcination temperatures generally negatively influenced catalytic performance, but with some significant exceptions among samples containing 10 and 20 mol% CuO. Calcination temperature, which produced the most active catalysts [13], was employed in this study. KIT-6 silica template was removed from the resulting solids by leaching twice with 2 M NaOH (Merck) at 50 °C. Traces of NaOH were removed by continuously washing samples with distilled water and centrifugation until pH value of the slurry reached 7. Finally, the mesoporous $CuO–CeO_2$ mixed oxide samples were dried overnight at 50 °C.

XRD diffractograms were recorded on a PANalytical X'pert PRO diffractometer using CuKα radiation (λ = 0.15406 nm). Catalyst samples were scanned in the 2θ ranges between 0.5 to 5° and 10 to 85° with 0.017° and 0.034° increments, respectively, and recording time of 100 s at each increment. N_2 adsorption/desorption measurements were performed using a Micromeritics ASAP 2020 MP/C apparatus. Prior to characterization, the samples were degassed in vacuum (4 μm Hg) at 300 °C. H_2-TPR/TPD measurements were carried out using a Micromeritics AutoChem II 2920 catalyst characterization system, with 250 mg of sample. For a detailed description of the utilized H_2-TPR/TPD protocol as well as determination of CuO dispersion and abundance of surface acidic sites refer to our previous study [13]. It should be pointed out that $CuO–CeO_2$ catalysts were prior to saturation with NH_3 reduced with 5% CO/He, contrary to reduction in 5% H_2/He, which was carried out prior to H_2-TPR/TPD experiments. Amounts of carbon formed on spent $CuO–CeO_2$ samples were determined using a DC-190 TOC apparatus (manufactured by Rosemount Analytical) by oxidizing the samples in purified air and quantifying the amount of produced CO_2 by comparison with a known standard (anhydrous Na_2CO_3). *In situ* DRIFTS measurements were performed on a PerkinElmer Spectrum 100 FTIR apparatus equipped with a DTGS detector. Calcined catalysts were placed inside porous ceramic cups and inserted into a high-temperature cell (DiffusIR® by PIKE Industries) with controlled atmosphere. Prior to scanning, the samples were purged in He flow for 1 h at 400 °C, which was followed by reduction in 5% CO/He for 1 h at the same temperature. To evaluate an influence of $CuO–CeO_2$ exposure to CO_2, calcined and purged (1 h at 400 °C in He) samples were exposed to 10% CO_2/He for 20 min at 105 °C. Afterwards, samples were purged with He and DRIFTS spectra were recorded at various times. Baseline and sample scans were obtained in the wavenumber range of 4000–450 cm^{-1} by accumulating 64 scans per spectrum at 4 cm^{-1} spectral resolution.

Water-gas shift reaction (WGSR) activity tests were carried out using a fixed-bed reactor system from PID Eng&Tech (model Microactivity Reference). 300 mg of a calcined catalyst was positioned inside the 9 mm ID Hastelloy C reactor between two quartz wool beads. Prior to reaction, the catalyst was reduced *in situ* in a 20% CO/He gas mixture at 400 °C for 1 h. Reaction temperature during activity tests was lowered in 25 °C decrements from 450 to 250 °C. At each temperature decrement, activity was monitored either for 7 or 15 h, which in total resulted in 95 h time on stream for each catalyst sample. Reactant gas mixture comprised of a stoichiometric ratio (1:1) of 94 ml/min CO (STP) and 94 ml/min water vapor. Distilled water (0.075 ml/min) was dosed by means of a Gilson 307 HPLC pump and evaporated in a heat box, operating at 180 °C, which is integrated in the reactor system. N_2 (50 ml/min) was used as an internal standard in the gas mixture to inspect GC consistency, and He (50 ml/min) as ballast gas. The total reactant flow was 288 ml (STP), which corresponds to GHSV of 23,560 h^{-1}. The employed reaction pressure was in all runs equal to 2.5 bar, due to pressure drop caused by the catalyst fixed bed and protective stainless steel frits inside the reactor system. Reaction products and remaining reactants were efficiently separated by means of HP Plot Q and Molesieve capillary columns, and qualitatively and quantitatively analyzed with an Agilent 7890 gas chromatograph equipped with TCD and FID detectors. The transfer line between the reactor system and gas chromatograph was heated to 200 °C using a heating tape in order to prevent water vapor condensation and to ensure acquisition of reliable data.

3. Results and discussion

3.1. Catalyst characterization

The nanocrystalline structure of investigated catalysts was identified by well-resolved diffraction peaks in the wide angle region of XRD patterns. As depicted in Fig. 1a, all recorded peaks

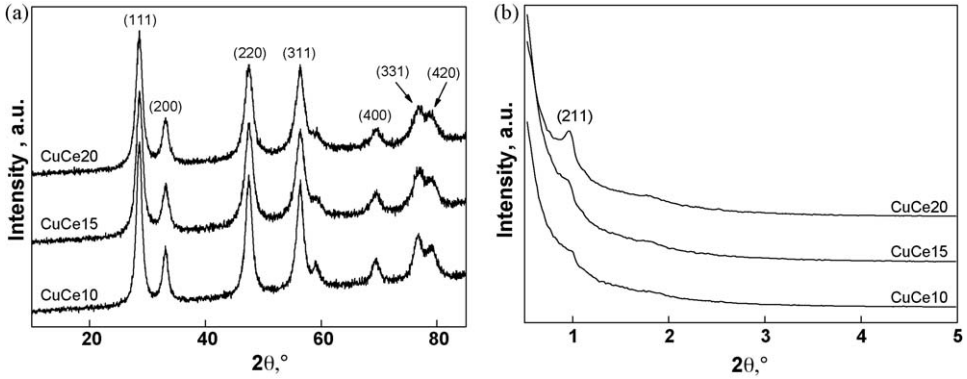

Fig. 1. (a) High angle XRD patterns of CuCe10, CuCe15 and CuCe20 samples; (b) low angle XRD diffractograms of catalysts.

Table 1
BET specific surface area and total pore volume of fresh and used samples, average CeO_2 crystallite size and CuO dispersion of CuO–CeO_2 catalyst samples.

Sample	Specific BET surface area (m^2/g)		Pore volume (cm^3/g)		[a]Average CeO_2 crystallite size (nm)	[a]CuO dispersion (%)
	Fresh	Used	Fresh	Used		
CuCe10	147	78	0.29	0.27	7.8	40.4
CuCe15	166	72	0.31	0.25	6.5	28.7
CuCe20	161	85	0.33	0.29	6.6	32.2

[a] Morphological properties of fresh catalyst samples.

could be attributed to the FCC fluorite CeO_2 phase (PDF data file 03-065-5923). Their positions agree closely with the literature data, indicating negligible solid solution formation [14]. Despite progressively higher CuO loading, no peaks belonging to any ordered copper phase was detected. These observations can be explained by taking into account the fact that CuO particles are extremely small and well dispersed on the CeO_2 (also proved by selective N_2O decomposition) and are consequently too small to be detected by XRD analysis. It is interesting to note that the average CeO_2 crystallite size (Table 1) corresponds to the very narrow pore size distribution window of the KIT-6 silica template (6–8.5 nm with a maximum at 7 nm), indicating that CuO and CeO_2 phases were encapsulated within the template pore structure, which limited their growth during the calcination process.

Low angle XRD analyses of CuCe materials were carried out in order to verify any similarity with structural symmetry of KIT-6 template. The presence of small characteristic XRD peaks at 2θ angle of 0.95° is a consequence of reflection from the (2 1 1) crystalline plane, which suggests cubic *Ia3d* symmetry also in the CuO–CeO_2 structure (Fig. 1b), thus reasonably confirming that the prepared CuCe solids are representatives of the KIT-6 pore structure.

By comparing BET surface area values of fresh CuCe catalysts (Table 1), it can be seen that it decreases with increasing calcination temperature, but was still 3–5 times higher than in the case when catalysts with the same chemical composition and thermal treatment were prepared by co-precipitation, sol–gel peroxide route and citric acid assisted synthesis methods [13,15]. A bimodal pore size distribution was observed in synthesized samples (Fig. 2). Pores centered around 4.1 nm are a consequence of template skeletal structure removal. Constant value of this maximum, corresponding to the KIT-6 wall thickness (calculated

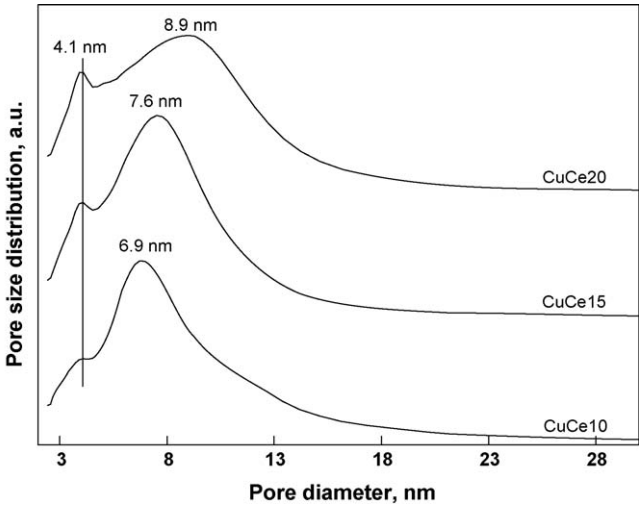

Fig. 2. Pore size distribution in CuCe10, CuCe15 and CuCe20 catalyst samples.

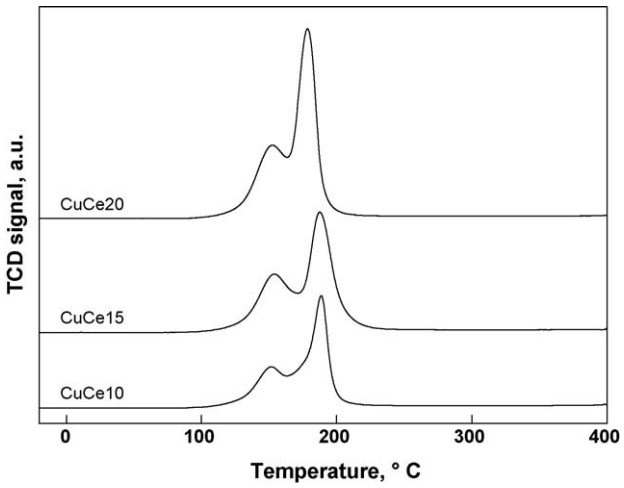

Fig. 3. H_2-TPR profiles of CuCe10, CuCe15 and CuCe20 catalysts.

to be 4.5 nm), indicates good stability of the CeO_2 framework and negligible phase migration during leaching and subsequent drying steps. Larger pores observed in the prepared CuCe solids can be attributed to the loading of CuO and CeO_2 precursors around pore wall junctures, and to a certain extent, precipitation outside the KIT-6 template. The second maximum shifts from 6.9 to 8.9 nm with increasing CuO loading, because smaller pores of the KIT-6 template get progressively filled and blocked at higher metal oxide loadings.

Results obtained by H_2-TPR/TPD experiments are presented in Fig. 3 and Table 2. Reduction of CuCe catalysts was in all cases initiated at around 100 °C with the first peak (attributed to the reduction of finely dispersed CuO and CeO_2 at the CuO–CeO_2 interface [13]) exhibiting a maximum at 155 °C. The second peak maximum was positioned at 180 °C for CuCe20 and at 190 °C for CuCe10 and CuCe15 samples, which is attributed to the reduction of bulk CuO. At temperatures around 225 °C, complete CuO reduction and partial CeO_2 reduction (14.4, 16.1 and 24.5% for CuCe10, CuCe15 and CuCe20 solids, respectively) were achieved. Reduction process of investigated mixed oxide samples takes place at temperatures, which are much lower than those of individual components (not shown) [15], thus exhibiting beneficial effect of strong interactions between oxide phases in CuO–CeO_2 catalysts on their redox properties.

The amount of H_2 consumed in the reduction process in all experiments surpassed the quantity needed for complete Cu^{2+} to Cu^0 reduction (Table 2), indicating considerable extent of CeO_2 support reduction and H_2 adsorption on the mixed oxide surface (evaluated by TPD experiments), which does not influence its reduction.

By increasing CuO content from 10 to 20 mol%, an increase in partial CeO_2 reduction from 14.4 to 24.5% was observed, indicating a positive influence of CuO on the formation of defects and oxygen mobility within the CeO_2 crystallite lattice, and consequently extent of its reducibility. A high fraction of reduced CeO_2 indicates that to some extent subsurface CeO_2 also underwent reduction.

Table 2
H_2-TPR/TPD data, partial CeO_2 reduction and amounts of desorbed NH_3 and CO_2 from CuO–CeO_2 catalyst samples.

Sample	TPR (ml/g) (STP)	TPD (ml/g) (STP)	Partial CeO_2 reduction (%)	Desorbed NH_3 ($\mu mol/m^2$) (STP)	Desorbed CO_2 ($\mu mol/m^2$) (STP)
CuCe10	30.8	9.3	14.4	1.24	1.78
CuCe15	41.5	10.7	16.1	0.89	2.22
CuCe20	49.8	9.5	24.5	0.92	2.41

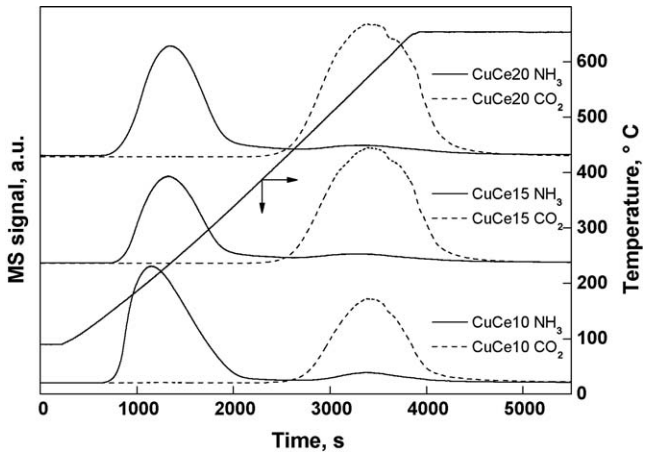

Fig. 4. NH_3 and CO_2 TPD profiles of CuCe10, CuCe15 and CuCe20 catalyst samples.

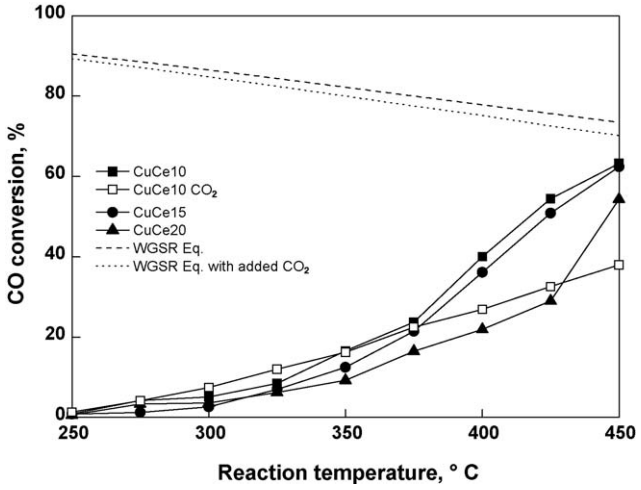

Fig. 5. Average CO conversion as a function of reaction temperature for CuCe10, CuCe15 and CuCe20 catalyst samples.

During surface acidity probing, considerable amounts of CO_2 desorbed from the surface of investigated samples were detected besides NH_3 (Fig. 4). It should be noted that CO_2 originates from the process of catalyst reduction with diluted CO, as it binds to the catalyst surface forming different carbonate species [16–18]. The amount of the latter increases with rising partial CeO_2 reduction and CuO loading (Table 2), indicating carbonate formation on CeO_2 surface [9,19,20] and CuO–CeO_2 contact area as a result of increased oxygen mobility/reactivity [16,18,21].

A bimodal NH_3-TPD curve was obtained for all tested samples (Fig. 4). The largest amount of NH_3 desorbed was observed for CuCe10 sample (Table 2), indicating the highest abundance of surface acid sites in this sample. Lower, but very similar quantities of NH_3 were desorbed from samples with 15 and 20 mol% CuO. The temperature range of NH_3 desorption (symmetrical peak between 140 and 430 °C with a maximum at around 240 °C) did not differ much for CuCe15 and CuCe20 materials, indicating very similar acid strength distribution in these two samples. In addition, a high temperature NH_3 desorption peak was detected at temperatures between 450 and 650 °C, whose amount was evaluated at 7.2 (CuCe15) and 6.2% (CuCe20) of total NH_3 consumption. On the other hand, CuCe10 sample exhibited a large asymmetric NH_3 desorption peak between 135 and 440 °C with a maximum at 210 °C, and another small peak (accounting for roughly 6% of total NH_3 consumption) between 480 and 650 °C with a maximum at 570 °C. The lower temperature peak exhibited a steep initial rise and pronounced tailing. Asymmetry of this peak indicates noticeable inhomogeneity of acid site strength with emphasis on weak acidic sites, which is probably connected to specific morphology of the CuCe10 sample.

3.2. WGSR activity tests

In Fig. 5, CO conversion as a function of reaction temperature, calculated using the following equation: $CO_{conversion} = 1 - (CO_{out}/CO_{in}) \times 100\,\%$, is depicted. Besides H_2 and CO_2, CH_4 as the only side product in the concentration range up to 1500 ppm was detected. This implies that the selectivity of investigated catalysts in excess of 99% was obtained over the entire temperature range.

Increasing WGS activity trend of tested CuO–CeO_2 catalysts coincides well with the abundance of surface acidic sites (CuCe10 > CuCe15 > CuCe20), indicating a positive influence and significant role of this parameter on the activity in the WGS reaction [22]. At the reaction temperature of 450 °C, CO conversions of 62, 61 and 54% were measured over CuCe10, CuCe15 and CuCe20 catalysts, respectively. Better WGS performance of CuCe10 catalyst in comparison to other two solids might also be a consequence of higher dispersion and consequently smaller size of CuO clusters (Table 1). Higher extent of CeO_2 reduction is an indication of enhanced oxygen mobility within the CeO_2 structure as a consequence of strong interactions between both metal oxide phases. It results in facile formation of oxygen vacancies, which aids the activation of reactants and thus significantly contributes to the WGS activity of CuO–CeO_2 solids [1]. In the case reported here, activity trends do not correlate with the extent of CeO_2 reduction, consequently it might be concluded that this parameter does not play a prevailing role in establishing WGS activity trends of these solids.

By increasing reaction temperature above 375 °C, some deactivation was observed for all CuCe samples in the investigated 7 or 15 h time on stream intervals. The highest extent of deactivation was observed for CuCe15 sample, which is in our opinion related to its structural modifications and sintering, since the utilized calcination temperature for this sample was 400 °C. A substantial drop in BET surface area (roughly 50%) was detected in all used CuCe samples after being tested in WGS reaction for 95 h (Table 1). Furthermore, differences in total pore volume of up to 20% and substantial differences in pore size distribution between fresh and used CuCe samples (not shown) were observed (the most prominent for CuCe15), thus confirming the contribution of sintering as a source of activity decline.

The presence of CO_2 in the feed gas stream was evaluated in terms of its negative influence on CO conversion throughout the whole tested temperature range (Fig. 5). It was suggested in our previous work [13] and confirmed by [17–20,23] that CO_2 causes the formation of different carbonate species on the ceria surface, which block active sites on CeO_2 and CuO–CeO_2 interface and additionally retard oxygen mobility within the CeO_2 crystallite lattice. As determined in this study (Fig. 4), carbonates formed during sample reduction in CO and WGS reaction exhibit extraordinary thermal stability and are consequently not actively involved in the process of oxygen transfer through the CeO_2 surface/structure. Furthermore CO_2 in the feed gas stream negatively influences the equilibrium CO conversion. WGS activity of the most active CuCe10 catalyst (Fig. 5) was investigated by replacing some of the He ballast gas with CO_2 (8.7% CO_2 in the feed gas stream), thus maintaining contact time as well as H_2O and CO concentrations in the feed gas constant, compared to experiments without CO_2 present. At reaction temperatures below 300 °C, negligible negative influence of added CO_2 was observed on WGS activity of tested catalyst (Fig. 5). By increasing the reaction

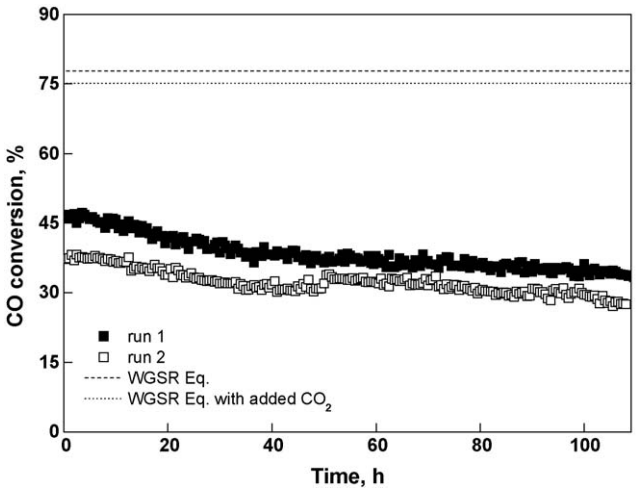

Fig. 6. Long-term stability tests of CuCe10 catalyst. Run 1: H_2O:CO = 1:1, $\Phi_{V,H_2O} = \Phi_{V,CO} = 94$ ml/min; $\Phi_{V,N_2} = \Phi_{V,He} = 50$ ml/min, $T = 400$ °C. Run 2: H_2O:CO = 1:1, $\Phi_{V,H_2O} = \Phi_{V,CO} = 94$ ml/min; $\Phi_{V,N_2} = 50$ ml/min, $\Phi_{V,CO_2} = \Phi_{V,He} = 25$ ml/min, $T = 400$ °C. After 50 h time on stream, CO_2 was replaced with He.

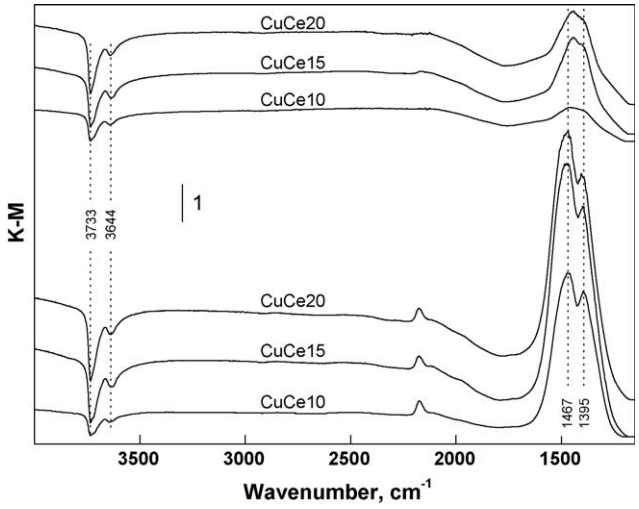

Fig. 7. DRIFTS spectra of: (a) calcined and degassed CuO–CeO_2 catalysts after reduction in 5% CO/He at 400 °C for 1 h (lower 3 spectra); (b) the same samples when heated to 700 °C in He (upper 3 spectra).

temperature above 375 °C, its negative influence became evident and the difference in measured CO conversions at the reactor outlet became progressively more prominent (38% vs. 62% CO conversion at 450 °C). It could be speculated that temperatures above 375 °C are needed for substantial formation of stable surface carbonates, which noticeably retard catalyst activity. It is described in more detail below that saturation of CuO–CeO_2 catalysts with CO_2 at 105 °C results in the formation of different surface carbonates and hydrogen carbonates, which can be removed in great majority by purging with He. Additionally, Marbán et al. [21] report that carbonates formed during the reaction are more strongly bound on the surface, compared to those produced by atmospheric exposure.

The most active CuCe10 catalyst sample was tested for long-term stability at the reaction temperature of 400 °C (Fig. 6). During the 110 h time on stream, CO conversion continuously decreased from 47 to 34% (run 1). The same experiment was repeated (run 2) but with a part of He replaced with CO_2. As shown in Fig. 6, lower initial CO conversion was observed (37%) in the case of added CO_2. As very similar slopes of CO conversion vs. time curves were observed in the absence of CO_2 in the feed gas stream (Fig. 6), this clearly demonstrates that the major source of deactivation of examined CuO–CeO_2 catalysts is sintering. After 50 h time on stream, CO_2 was replaced with He and CO conversion instantly rose from 31 to 34%. The observed activity increase can be attributed to the decrease in competitive adsorption between CO and CO_2 and WGS reaction equilibrium. The remaining difference in CO conversion between runs 1 and 2 from 50 h time on stream onward can be attributed to additional formation of surface carbonates as a result of CO_2 present in the feed gas stream, alteration of acidic/basic properties and more pronounced sintering during the initial stage of reaction.

To evaluate additional deactivation sources, carbon formation on spent CuCe10 catalysts was evaluated. It was discovered that some coking of catalyst occurred during long-term stability tests (Fig. 6). The amount of deposited carbon (0.39 wt.% for run 1 and 0.34 wt.% for run 2) depends on the composition of feed gas stream. Addition of CO_2 slightly retarded coking, but enhanced catalyst sintering (BET surface areas of spent CuCe10 catalysts were found to be 89 m^2/g for run 1 and 75 m^2/g for run 2).

3.3. DRIFTS experiments

It was shown by numerous authors that pure CeO_2 or CeO_2 doped with either precious metals (Au, Pt, Pd) [16,18–20,23], or transition metals such as Cu [9,17] exhibits high affinity toward the formation of various surface carbonates, formates, etc., when exposed to CO, CO/H_2 or CO/H_2O gas mixtures under PROX and WGS reaction conditions. To identify carbonate species formed on the surface of calcined CuO–CeO_2 catalysts during the reduction in 5% CO/He at 400 °C for 1 h, DRIFTS experiments were carried out (Fig. 7).

Assignment of specific bands to the various vibrational modes of surface species is provided in Table 3. As one can see, extensive formation of monodentate carbonates, probably as a result of CO incorporation into the structure of CuO–CeO_2 via the following reaction: $Ce^{4+} - O_2^- - Cu^+ - CO \rightarrow Ce^{3+} - CO_3^- - Cu^{2+}$, was identified when characteristic band positions (ν_s(COO) at 1395 and ν_{as}(COO) at 1467 cm^{-1}) were compared to the literature data.

Besides intense peaks in the 1700–1200 cm^{-1} region, attributed to monodentate carbonates, sharp negative peaks were also observed in the 3800–3600 cm^{-1} region, which were attributed to stretching frequencies of bridge bonded hydroxyl groups (3644 cm^{-1}) and isolated hydroxyl groups (3733 cm^{-1}).

The reason behind negative bands at characteristic hydroxyl stretching frequencies lies in the inability of degassing procedure

Table 3
Positions of DRIFTS peaks and their assignment.

Potential assignment	Our values (cm^{-1})	Literature values (cm^{-1})
Monodentate carbonate	1395, 1467, 1317, 1340, 1474, 1536	1478 [9]; ν_{as}(COO) at 1530–1470 with symmetric ν_s(COO) vibrations at 1370–1300 [16]; 1478, 1399 [17]; 1420 [18]
Bidentate carbonate	1554, 1608	1554, 1325, 1583, 1297, with overtone at 2880 [9]; ν_{as}(COO) at 1220–1270, ν(CO) at 1670–1530 [16]; 1586, 1297 [17]; 1287, 1291 [18]
Hydroxyl groups	3644, 3733	3663, 3696, 3683, 3655, 3681 [23]; 3712–3690 [9]; 3727 isolated hydroxyls [16]; 3647 bridged [18]
Hydrogen carbonates	1217, 1391, 3618	1216, 1399 [9]; 3619 OH stretching vibration of the HCO_3- functional group [19]

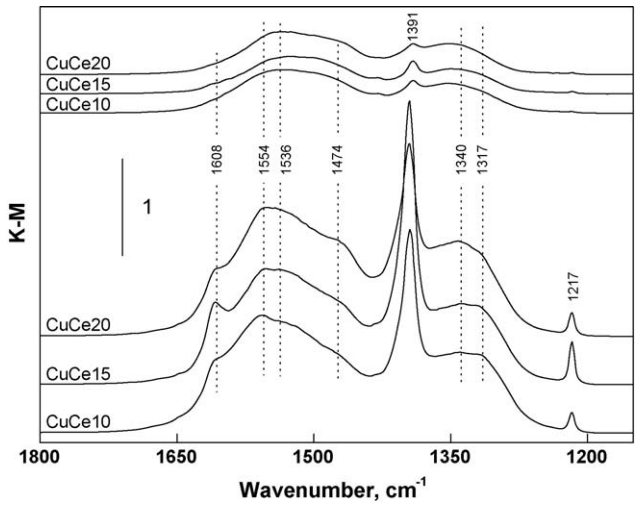

Fig. 8. DRIFTS spectra of: (a) calcined CuO–CeO_2 catalysts after saturation with CO_2 at 105 °C for 20 and 20 min purging with He (lower 3 spectra); (b) after purging with He at 105 °C for 100 min (upper 3 spectra).

of calcined CuCe samples (400 °C for 1 h in He flow) prior to reduction in CO, to completely remove surface OH groups. This reveals great affinity of tested materials toward H_2O adsorption and high thermal stability of surface hydroxyl groups. During the *in situ* catalyst reduction, CO reacts with surface hydroxyl groups; formates are formed, decomposed and desorbed from the catalyst surface (no bands which could be attributed to these species were found in the expected 2800–3000 cm^{-1} range). Complete removal of hydroxyl groups during CO reduction (or catalyst activation step) can be confirmed with the fact that negative bands attributed to these species, do not change in intensity when the temperature was raised from 400 to 700 °C. Increasing the temperature also caused complete disappearance of bands at 2173 cm^{-1} and greatly reduced bands in the 1700–1200 cm^{-1} range, ascribed to monodentate carbonates (Fig. 7). This observation is in agreement with the results of CO_2-TPD runs (Fig. 4). Extreme conditions, needed for decomposition and removal of surface carbonates indicate their extraordinary stability and great affinity of tested CuCe materials to chemisorb CO at elevated temperatures. It also supports findings of Alexeev et al. [16] and Denkwitz et al. [18], who claim that monodentate are by far most stable carbonate species formed on the CuO–CeO_2 materials. Finally, the above-described findings confirm that negligible decomposition of carbonates formed via the CO insertion into the catalyst structure, would be expected at typical WGSR conditions.

On the other hand, exposure of calcined and degassed CuCe catalysts to 10% CO_2/He at 105 °C for 20 min resulted in the formation of various surface carbonate and hydrogen carbonate species. In the presented DRIFTS spectra (Fig. 8), several sharp and intense peaks along with some broader ones can be discerned in the 1700–1200 cm^{-1} region, which can be attributed to monodentate carbonate (ν_s(COO): 1317, 1340 cm^{-1}; ν_{as}(COO): 1474, 1536 cm^{-1}), bidentate carbonate (ν_{as}(-COO): 1554 and 1608 cm^{-1}) and hydrogen carbonate (1217 and 1391 cm^{-1}) species.

Peaks attributed to same vibrational/stretching modes of same functional group (Fig. 8) are located at different wavenumbers as a result of great inhomogeneity of catalyst surface (redox state and different coordination of exposed surface atoms) as well as inductive and mesomeric effects [24]. Further purging of CO_2-saturated CuCe catalyst samples with He at 105 °C resulted in noticeable decrease of all observed bands disclosing low thermal stability and bonding strength of these species. The above results show that CO insertion into the structure of CuO–CeO_2 solids results in the formation of strongly bound carbonate species on the catalyst surface. This process occurs either during catalyst pretreatment/activation step or simultaneously during the WGS reaction, and contributes (besides sintering effect) to a decline in catalyst activity. Similar to our observation, gradual decrease of catalyst activity due to carbonate formation induced by CO presence in the gas phase was observed by Marbán et al. [21] who investigated PROX reaction over CuO–CeO_2 catalysts prepared by means of SACOP method.

4. Conclusions

The following conclusions can be drawn on the basis of gathered experimental data:

- The obtained catalysts exhibit very high BET specific surface area and pore volume. Their ordered structure resembles *Ia3d* symmetry as a result of their incorporation inside the pore system of KIT-6 template during calcination procedure.
- H_2-TPR/TPD experiments revealed facile and extensive reducibility of CeO_2, along with complete reducibility of CuO, indicating high oxygen mobility within the CeO_2 sublattice, as a result of strong electronic interactions between both metal oxide phases. Increasing CuO content from 10 to 20 mol% leads to a decreased CuO dispersion and lower abundance of surface acidic sites.
- WGSR activity tests revealed high activity of investigated CuCe catalysts under utilized reaction conditions with activity trends following the trend of surface acidic site abundance and CuO dispersion (CuCe10 > CuCe15 > CuCe20). Addition of CO_2 to the feed gas stream resulted in lower CO conversion at reaction temperatures above 350 °C, as a result of competitive adsorption with CO, unfavorable WGS reaction equilibrium and enhanced sintering.
- Insertion of CO into the lattice of CuO–CeO_2 solids during activation and reaction steps leads to extensive formation of monodentate carbonates, which cannot be removed from the catalyst surface under utilized WGS reaction conditions.

Acknowledgement

The authors gratefully acknowledge the financial support of the Ministry of Education, Science and Technology of the Republic of Slovenia through Research program No. P2-0152.

References

[1] H. Kušar, S. Hočevar, J. Levec, Appl. Catal. B 63 (2006) 194.
[2] F. Huber, Z. Yu, J.C. Walmsley, D. Chen, H.J. Venvik, A. Holmen, Appl. Catal. B 71 (2007) 7.
[3] G. Avgouropoulos, T. Ioannides, Appl. Catal. A 244 (2003) 155.
[4] F. Mariño, C. Descorme, D. Duprez, Appl. Catal. B 58 (2005) 175.
[5] W. Liu, M. Stephanopoulos, J. Catal. 153 (1995) 304.
[6] P. Bera, K.R. Priolkar, P.R. Sarode, M.S. Hegde, S. Emura, R. Kumashiro, N.P. Lalla, Chem. Mater. 14 (2002) 3591.
[7] J. Papavasiliou, G. Avgouropoulos, T. Ioannides, Appl. Catal. B 69 (2007) 226.
[8] W. Shen, X. Doug, Y. Zhu, H. Chen, J. Shi, Micropor. Mesopor. Mater. 85 (2005) 157.
[9] D. Gamarra, A. Martínez-Arias, J. Catal. 263 (2009) 189.
[10] J. Zhu, Q. Gao, Z. Chen, Appl. Catal. B 81 (2008) 236.
[11] S.C. Laha, R. Ryoo, Chem. Commun. (2003) 2138.
[12] A. Rumplecker, F. Kleitz, E.-L. Salabas, F. Schüth, Chem. Mater. 19 (2007) 485.
[13] P. Djinović, J. Batista, A. Pintar, Appl. Catal. A 347 (2008) 23.
[14] V.K. Pecharsky, P.Y. Zavalij, Fundamentals of Powder Diffraction and Structural Characterization of Materials, Springer, 2005, pp. 164.
[15] A. Pintar, J. Batista, S. Hočevar, J. Colloid Interface Sci. 307 (2007) 145.
[16] O.S. Alexeev, S. Krishnamoorthy, C. Jensen, M.S. Ziebarth, G. Yaluris, T.G. Roberie, M.D. Amiridis, Catal. Today 127 (2007) 189.
[17] A. Martínez-Arias, A.B. Hungría, G. Munuera, D. Gamarra, Appl. Catal. B 65 (2006) 207.
[18] Y. Denkwitz, A. Karpenko, V. Plzak, R. Leppelt, B. Schumacher, R.J. Behm, J. Catal. 246 (2007) 74.

[19] O. Pozdnyakova, D. Teschner, A. Wootsch, J. Kröhnert, B. Steinhauer, H. Sauer, L. Toth, F.C. Jentoft, A. Knop-Gericke, Z. Paál, R. Schlögl, J. Catal. 237 (2006) 1.
[20] K.G. Azzam, I.V. Babich, K. Seshan, L. Lefferts, J. Catal. 251 (2007) 153.
[21] G. Marbán, I. López, T. Valdés-Solís, Appl. Catal. A (2009), doi:10.1016/j.apcata.2009.04.014.
[22] P. Djinović, J. Levec, A. Pintar, Catal. Today 138 (2008) 222.
[23] T. Tabakova, F. Boccuzzi, M. Manzoli, D. Andreeva, Appl. Catal. A 252 (2003) 385.
[24] D. Lin-Vien, N.B. Colthup, W.G. Fateley, J.G. Grasselli, The Handbook of Infrared and Raman Characteristic Frequencies of Organic Molecules, Academic Press, 1991, pp. 118–122.